Molecular basis of transmembrane signalling by sensory rhodopsin II–transducer complex

Valentin I. Gordeliy*†, Jörg Labahn*, Rouslan Moukhametzianov*†, Rouslan Efremov*†, Joachim Granzin*, Ramona Schlesinger*, Georg Büldt*, Tudor Savopol§||, Axel J. Scheidig§, Johann P. Klare§ & Martin Engelhard§

* *Research Centre Jülich, Institute of Structural Biology (IBI-2), 52425 Jülich, Germany*
† *Centre for Biophysics and Physical Chemistry of Supramolecular Structures, MIPT, 141700, Moscow District, Russia*
§ *Max-Planck-Institut für Molekulare Physiologie, Otto Hahn Str. 11, 44227 Dortmund, Germany*
|| *Present address: Carol Davila Medical and Pharmaceutical University, POB15-205 Bucharest, Romania.*

Microbial rhodopsins, which constitute a family of seven-helix membrane proteins with retinal as a prosthetic group, are distributed throughout the Bacteria, Archaea and Eukaryota[1–3]. This family of photoactive proteins uses a common structural design for two distinct functions: light-driven ion transport and phototaxis. The sensors activate a signal transduction chain similar to that of the two-component system of eubacterial chemotaxis[4]. The link between the photoreceptor and the following cytoplasmic signal cascade is formed by a transducer molecule that binds tightly and specifically[5] to its cognate receptor by means of two transmembrane helices (TM1 and TM2). It is thought that light excitation of sensory rhodopsin II from *Natronobacterium pharaonis* (SRII) in complex with its transducer (HtrII) induces an outward movement of its helix F (ref. 6), which in turn triggers a rotation of TM2 (ref. 7). It is unclear how this TM2 transition is converted into a cellular signal. Here we present the X-ray structure of the complex between *N. pharaonis* SRII and the receptor-binding domain of HtrII at 1.94 Å resolution, which provides an atomic picture of the first signal transduction step. Our results provide evidence for a common mechanism for this process in phototaxis and chemotaxis.

Crystallization of the receptor–transducer complex, a member of the two-component signalling cascade (Fig. 1), has been achieved successfully using a shortened transducer (residues 1–114; *N. pharaonis* $HtrII_{114}$) comprising the two transmembrane helices (TM1 and TM2) and an additional small cytoplasmic fragment. This construct satisfies the properties of an appropriate model system for the native receptor–transducer complex as indicated by a low dissociation constant ($K_d \approx 100$ nM, S. Hippler-Mreyen, unpublished data) and by its capability to inhibit the inherent proton pump activity of SRII, as was shown for a larger transducer fragment (G. Schmies, unpublished data) and the full-length transducer[8,9]. These data and those establishing a functional signal transfer from receptor to transducer[7] indicate that $HtrII_{114}$ forms a functionally unimpaired complex with its cognate receptor SRII.

The thin orange crystals of SRII in complex with $HtrII_{114}$ grown in lipidic cubic phase[10] displayed an orthorhombic shape of about 140 μm in size and diffracted to 1.8 Å. The asymmetric unit contains one complex. The expected dimer of the complex is formed by a crystallographic two-fold rotation axis, which is located in the middle of four transmembrane helices: TM1, TM2, TM1′, TM2′ (where a prime indicates the right-hand complex; Fig. 2a). The transmembrane helices F and G of the receptor are in contact with the helices of the transducer. The overall X-ray structure is in good agreement with a recently published model of the receptor–transducer complex deduced from electron paramagnetic resonance (EPR) measurements[7].

The structure of SRII complexed with its transducer is markedly similar to that of the receptor alone including the retinal conformation[11,12]. Obviously, the binding of the transducer to helices F and G hardly interferes with the side-chain arrangement of the receptor. A notable exception is found for Tyr 199. The aromatic plane of Tyr 199 has turned in the complex by about 90° and is now pointing into the direction of TM2 where its phenolic group forms a hydrogen bond to Nδ(2)-Asn 74 (2.8 Å). An interaction of Tyr 199 with the transducer has been proposed previously[12]. It should be mentioned that a chloride ion, identified by ref. 11, close to the guanidinium group of Arg 72 is clearly absent in the present structure. The crystallization conditions used by this study (low pH and high NaCl concentration) favour the uptake of a chloride ion and therefore can explain the differences. The natural habitat of *N. pharaonis* (pH > 9) does not support the binding of a chloride ion to SRII.

The interface between receptor and transducer is formed mainly by van der Waals (vdW) contacts and only a few hydrogen bonds. Whereas the straight TM2 is oriented parallel to helix G of the receptor, TM1 is kinked at Gly 37 and bends away from the receptor. Thus, a crevice (formed by helices A, G, TM2 and TM1) opens to the cytoplasmic surface (Fig. 2a), which might harbour the back-folded amino terminus of TM1, as residual electron densities suggest. Although only van der Waals contacts are observed between the four transducer helices themselves, defined cross-connections are observed between receptor and transducer. The F–G loop region affixes the transducer by several contacts as well as by three hydrogen bonds between Thr 189 (SRII), Glu 43 (TM1) and Ser 62 (TM2) (Fig. 3). A second anchor point is observed in the middle of the membrane where, as mentioned above, the phenolic hydroxyl of Tyr 199 (helix G) bridges to Asn 74 (TM2). A view from the cytoplasm down the binding domain (Fig. 4a) reveals that closer contacts are between helix G and TM2, fixating these two transmembrane helices to one another. There are twice as many van der Waals contacts between helices G and TM2 than between F and TM2. The closer packing between G and TM2 can be quantified by an average van der Waals distance of 4.06 Å in comparison to a value of 4.22 Å between F and TM2 (Fig. 4b). The four helices of the

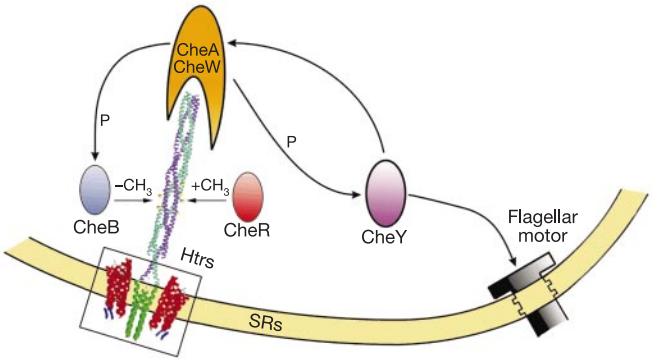

Figure 1 Two-component signalling cascade. The activation of the transducer HtrII by its receptor SRII leads to a conformational change of TM2 that propagates to the tip of the coiled-coil cytoplasmic domain (structure taken from ref. 31). The next steps in the signalling cascade involve—in analogy to the bacterial sensory system[20]—the homodimeric histidine kinase CheA, the coupling protein CheW, and the response regulators/aspartate kinases CheY and CheB. Phosphorylated (P) CheY functions as a switch factor of the flagellar motor. CheB (a methylesterase) together with CheR (a methyltransferase) are involved in the adaptation processes of the bacteria. The box highlights the receptor–transducer complex reported in the present study. SR, sensory rhodopsin.

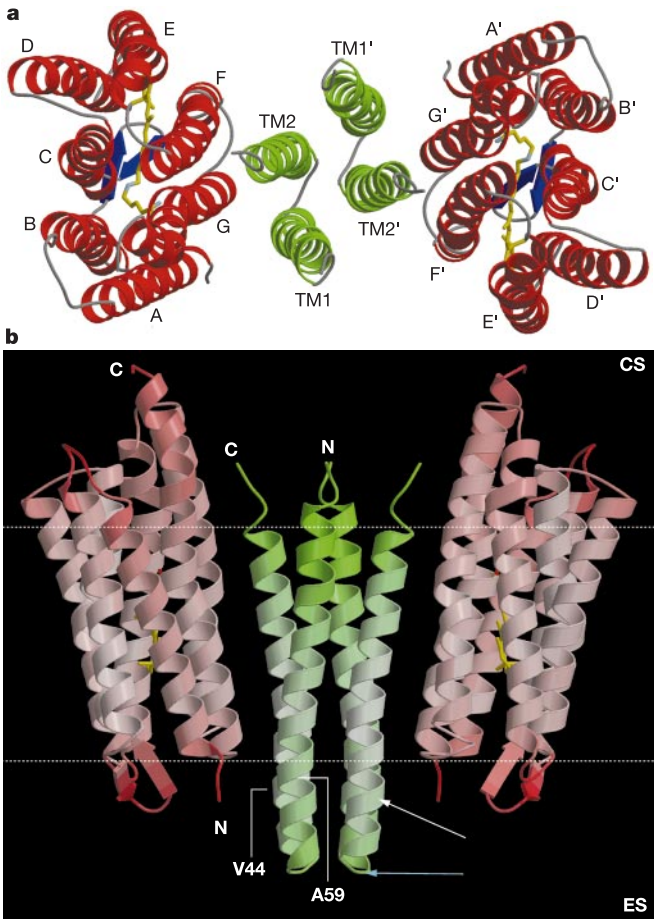

Figure 2 Fold of the receptor–transducer complex **a**, Ribbon diagram of the top view from the cytoplasmic side. α-Helices are in red for the receptor and green for the transducer; β-strands are in blue and coils in grey. The labels of the symmetry related complex are marked by a prime. The crystallographic symmetry axis is located between TM1–TM2 and TM1′–TM2′. **b**, Side view of the complex. The complex is coloured according to *B*-factor mobility: light red/green (less mobile), dark red/green (mobile). ES, extracellular side; CS, cytoplasmic side. The dotted white lines confine the major hydrophobic core of the proteins. Of note, the actual membrane boundary will not follow these straight lines. The arrows indicate the shortened stalk in HtrI (white) and the site where the helices α1 and α4 of the chemoreceptor domain of *H. salinarum* HtrII are attached to the transmembrane helices TM1 and TM2 (blue). All figures were generated with MOLSCRIPT and Raster3D.

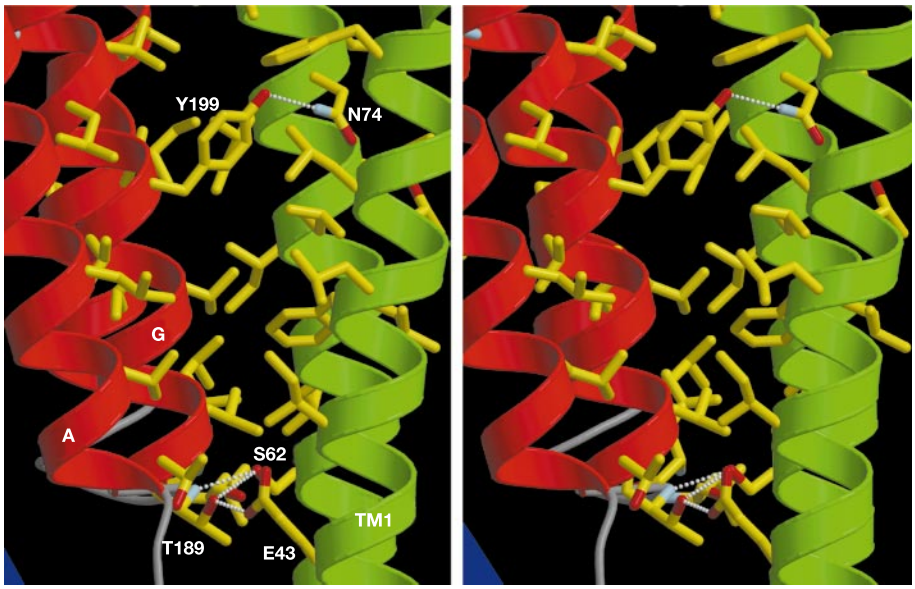

Figure 3 Stereo view of the hydrogen bonds and van der Waals contacts between receptor (α-helices in red) and transducer (α-helices in green). The residues that are involved in hydrogen bonds are labelled.

transducer in the dimer are packed against each other, thereby intercalating their bulky hydrophobic side chains.

Further insight into the structure of the receptor–transducer complex is gained if the structure is viewed perpendicular to the membrane. Most notably, the four helices of the transducer extend beyond the extracellular side by about three helical turns, comprising residues 44–59 (Fig. 2b). This sequence is missing in HtrI from *Halobacterium salinarum*, as obtained from a sequence alignment with *N. pharaonis* HtrII, but is repeated at the N-terminal end of TM2 in *H. salinarum* HtrII (ref. 13). Notably, *H. salinarum* HtrII not only transmits the signal from the photoreceptor SRII but also operates as a chemoreceptor[14]. This function is conferred by a serine-binding domain that is inserted in front of the sequence forming the stalk. Crystal structures of the ligand-binding domain of homologous eubacterial aspartate receptors display two extended helices in the dimer (α4 and α4′), which could connect to a structural element like the stalk[15]. The observation of different degrees of periplasmic domain excision is in line with the evolution of the four archetypical halobacterial rhodopsins, which has been explained by two gene duplication events[16]. According to this hypothesis a proto-chemoreceptor gene has been acquired by the proto-sensor gene after the first duplication step.

The temperature factors along the transducer and the receptor helices F and G increase from the centre to the cytoplasmic side of the proteins (Fig. 2b). Furthermore, the structure of TM2 ends with Leu 82, leaving residues 83–114 in multiple conformations, although they are necessary for receptor binding (S. Hippler-Mreyen, personal communication). An increased flexibility in this part of the molecule would facilitate the shift between the active and inactive conformations, which should be thermodynamically close to each other.

As shown previously, light excitation of *N. pharaonis* SRII triggers an outward movement of the cytoplasmic part of helix F (first observed for bacteriorhodopsin[17,18]). It was proposed that this conformational change induces a clockwise rotation of TM2 if seen from the cytoplasmic side (ref. 7). On the other hand, the binding of ligands to the chemotaxis receptor domain generates a piston-type sliding of one of its helices (α4) of about 1.6 Å (although a small rotation can not be excluded)[19,20]. It was proposed that this conformational change propagates along TM2—which is joined to α4—towards the inside of the cell (reviewed by ref. 20). As

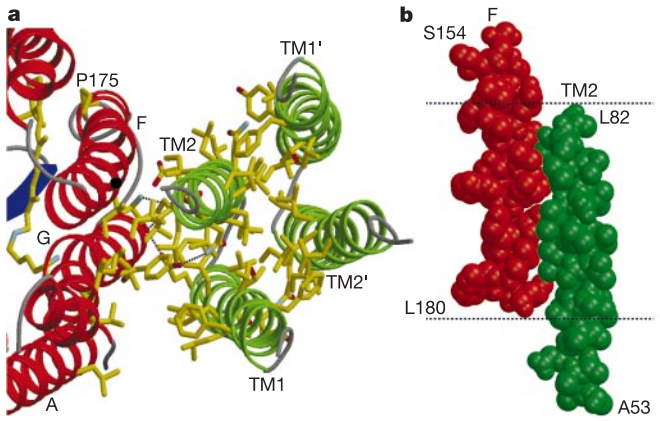

Figure 4 Interactions between SRII and HtrII. **a**, View from the cytoplasm down the binding domain. Several residues involved in the van der Waals contact are shown. The transducer helices are coloured green. The black dot on helix F marks the equivalent height in helix F corresponding to the start of helix TM2. **b**, Space-filling model showing close contact between helix F and TM2 as viewed from the direction of helix G. Starting and ending amino acids are shown. The black dashed lines confine the hydrophobic core as in Fig. 2b.

Table 1 **X-ray crystallographic data**

Data collection*	
Space group	$P2_12_12$
Cell dimensions (Å)	124.30, 46.96, 53.84
Unique reflections; average redundancy	23,156; 3.5
Completeness (%)	94.7 (77.3)
R_{merge} (%)	6.2 (39.4)
$I/\sigma(I)$	5.5 (1.7)
Refinement†	
R_{work}; R_{free} (%)	22.8; 25.8
Average *B*-factor (Å^2); No. of atoms	32.2; 2,187
r.m.s. deviation: bonds (Å); angles (°)	0.009; 1.07

$R_{merge} = \sum_h \sum_i |I_i(h) - \langle I(h)\rangle| / \sum_h \sum_i I_i(h)$, where $I_i(h)$ is the *i*th measurement and $\langle I(h)\rangle$ is the mean of all measurements of $I(h)$. Numbers in parentheses indicate the value for the outermost shell. For calculation of R_{free}, 5% of the reflections were reserved.
$R = \sum_h ||F_o(h)| - |F_c(h)|| / \sum_h |F_o(h)|$; where $|F_o|$, $|F_c|$ are observed and calculated structure factor amplitudes.
*Data were collected at beamline ID14-1 of ESRF at wavelength 0.934 Å.
†Residue range: SRII, 1–225; Htr, 24–82.

the *H. salinarum* SRII–HtrII complex displays dual functionality, a common mechanism of transmembrane signalling for phototaxis and chemotaxis should exist. The crystal structure of *N. pharaonis* SRII–HtrII reveals features that bear significance for the process of signal propagation across the membrane.

The present structure and the observation that the flap-like movement of helix F induces a rotation of the cytoplasmic end of TM2 (refs 6, 7), gives rise for a probable mechanism of transmembrane signalling. Helix F contains a proline residue (Pro 175; Fig. 4a) at an equivalent depth as Tyr 199 (Figs 3 and 4a), which could function as a hinge for the light-activated movement of helix F (a similar role has been proposed for Pro 185 in bacteriorhodopsin[21]). If the outward bending of helix F is in the same direction as observed for bacteriorhodopsin, it should collide tangentially with TM2 (Figs 2a and 4), thereby inducing its rotary motion. A primary piston-like transition of TM2 seems unlikely because the structure shows that TM2 has numerous side-chain intercalations with helix G and TM1 (see above and Fig. 4a). As TM2 is anchored to helix G, the rotation might occur around an axis located between the two helices. Rotation might involve an unwinding of the cytoplasmic coiled-coil helices (Fig. 1) as was observed for the γ-subunit of the F_1F_0-ATP synthase rotary motor[22]. As mentioned above, signal transfer from chemoreceptors and photoreceptors should follow similar mechanisms. A screw-like movement would satisfy both observations of a piston as well as a rotary motion of TM2. It should be noted that the initial ligand-induced shift of TM2 (whether a piston, rotary, or screw-type motion) might just be the trigger to shift the equilibrium from the inactive to the active state of the transducer, thereby producing a similar final conformation, recognized by the His kinase CheA.

Another interesting aspect derived from the structure of the receptor–transducer complex concerns the negative cooperativity observed not only for chemoreceptors but also, for example, for tyrosine kinase receptors such as the insulin receptor (discussed by ref. 23). Before excitation, the environment of the two helices TM2 and TM2′ appears to be the same (Fig. 2a). After excitation of one receptor molecule the corresponding TM2 will move, thus changing the environment of the other TM2, which might inhibit its equivalent movement. Therefore, the photoreceptors would show the negative cooperativity characteristic for chemoreceptors.

The high-resolution structure of the receptor–transducer complex provides the foundation for understanding transmembrane signalling on a molecular level. It has now become possible to solve the structure of intermediates, as has been done for bacteriorhodopsin. This new information will be of significance not only for bacterial phototaxis and chemotaxis but also for other dimeric receptors, which might lead finally to a general model of transmembrane signal transduction. □

Methods

Protein preparation

The genes of *N. pharaonis* SRII and the carboxy terminal truncated transducer (1–114) were cloned into a pET27bmod expression vector[24] with a C-terminal ×7 His tag, respectively. Proteins were expressed in *Escherichia coli* strain BL21 (DE3), and purified as described[25,26]. After removal of imidazol by diethyl-aminoethyl chromatography, SRII-His and $HtrII_{114}$-His were mixed in a 1:1 ratio, followed by reconstitution into purple membrane (the bacteriorhodopsin containing membrane patches of *H. salinarum*) lipids[7] (protein to lipid ratio 1:35). After filtration, the reconstituted proteins were pelleted by centrifugation at 100,000*g*. For resolubilization, the samples were resuspended in a buffer containing 2% *n*-octyl-β-D-glucopyranoside and shaken for 16 h at 4 °C in the dark. The resolubilized complex was isolated by centrifugation at 100,000*g*.

Crystallization, structure determination and refinement

We added the solubilized complex in crystallization buffer (150 mM NaCl, 25 mM Na/KPi, pH 5.1, 0.8% *n*-octyl-β-D-glucopyranoside) to the lipidic phase, formed from monovaccenin (Nu-Chek Prep). Precipitant was 1 M salt Na/KPi, pH 5.6. Crystals were grown at 22 °C.

X-ray diffraction data were collected at beamline ID14-1 of the European Synchrotron Radiation Facility (ESRF), Grenoble, France, using a Quantum ADSC Q4R CCD (charge-coupled device) detector. Data were integrated using MOSFILM[27] and SCALA[28]. Molecular replacement using MOLREP[28] to phase a polyalanine model (from Protein Data Bank accession number 1JGJ (ref. 12)) gave a unique solution ($R = 0.568$, correlation coefficient $C = 0.357$) at 2.9 Å. After inserting side chains for SRII, the helices of HtrII were found ($R = 0.329$, $C = 0.711$). Simulated annealing, positional refinement and temperature factor refinement were performed in CNS[29]; model rebuilding was carried out in O[30] (Table 1).

Received 9 May; accepted 16 July 2002; doi:10.1038/nature01109.

1. Oesterhelt, D. & Stoeckenius, W. Rhodopsin-like protein from the purple membrane of *Halobacterium halobium*. *Nature* **233,** 149–152 (1971).
2. Bieszke, J. A. *et al.* A eukaryotic protein, NOP-1, binds retinal to form an archaeal rhodopsin-like photochemically reactive pigment. *Biochemistry* **38,** 14138–14145 (1999).
3. Béjà, O. *et al.* Bacterial rhodopsin: evidence for a new type of phototrophy in the sea. *Science* **289,** 1902–1906 (2000).
4. Rudolph, J. & Oesterhelt, D. Deletion analysis of the che operon in the archaeon *Halobacterium salinarium*. *J. Mol. Biol.* **258,** 548–554 (1996).
5. Zhang, X. N., Zhu, J. & Spudich, J. L. The specificity of interaction of archaeal transducers with their cognate sensory rhodopsins is determined by their transmembrane helices. *Proc. Natl Acad. Sci. USA* **96,** 857–862 (1999).
6. Wegener, A. A., Chizhov, I., Engelhard, M. & Steinhoff, H. J. Time-resolved detection of transient movement of helix F in spin- labelled pharaonis sensory rhodopsin II. *J. Mol. Biol.* **301,** 881–891 (2000).
7. Wegener, A. A., Klare, J. P., Engelhard, M. & Steinhoff, H. J. Structural insights into the early steps of receptor-transducer signal transfer in archaeal phototaxis. *EMBO J.* **20,** 5312–5319 (2001).
8. Schmies, G. *et al.* Electrophysiological characterization of specific interactions between bacterial sensory rhodopsins and their transducers. *Proc. Natl Acad. Sci. USA* **98,** 1555–1559 (2001).
9. Sasaki, J. & Spudich, J. L. Proton circulation during the photocycle of sensory rhodopsin II. *Biophys. J.* **77,** 2145–2152 (1999).
10. Landau, E. M. & Rosenbusch, J. P. Lipidic cubic phases—a novel concept for the crystallization of membrane proteins. *Proc. Natl Acad. Sci. USA* **93,** 14532–14535 (1996).
11. Royant, A. *et al.* X-ray structure of sensory rhodopsin II at 2.1-Å resolution. *Proc. Natl Acad. Sci. USA* **98,** 10131–10136 (2001).
12. Luecke, H. *et al.* Crystal structure of sensory rhodopsin II at 2.4 Å: insights into colour tuning and transducer interaction. *Science* **293,** 1499–1503 (2001).
13. Zhang, W. S., Brooun, A., Mueller, M. M. & Alam, M. The primary structures of the archaeon *halobacterium salinarium* blue light receptor sensory rhodopsin II and its transducer, a methyl-accepting protein. *Proc. Natl Acad. Sci. USA* **93,** 8230–8235 (1996).
14. Hou, S. B. *et al.* Sensory rhodopsin II transducer HtrII is also responsible for serine chemotaxis in the archaeon *halobacterium salinarum*. *J. Bacteriol.* **180,** 1600–1602 (1998).
15. Yeh, J. I. *et al.* High-resolution structures of the ligand binding domain of the wild-type bacterial aspartate receptor. *J. Mol. Biol.* **262,** 186–201 (1996).
16. Ihara, K. *et al.* Evolution of the archaeal rhodopsins: evolution rate changes by gene duplication and functional differentiation. *J. Mol. Biol.* **285,** 163–174 (1999).
17. Koch, M. H. J. *et al.* Time-resolved X-ray diffraction study of structural changes associated with the photocycle of bacteriorhodopsin. *EMBO J.* **10,** 521–526 (1991).
18. Subramaniam, S., Gerstein, M., Oesterhelt, D. & Henderson, R. Electron diffraction analysis of structural changes in the photocycle of bacteriorhodopsin. *EMBO J.* **12,** 1–8 (1993).
19. Lynch, B. A. & Koshland, D. E. Jr Structural similarities between the aspartate receptor of bacterial chemotaxis and the trp repressor of *E. coli*. Implications for transmembrane signaling. *FEBS Lett.* **307,** 3–9 (1992).
20. Falke, J. J. & Hazelbauer, G. L. Transmembrane signaling in bacterial chemoreceptors. *Trends Biochem. Sci.* **26,** 257–265 (2001).
21. Gerwert, K., Hess, B. & Engelhard, M. Proline residues undergo structural changes during proton pumping in bacteriorhodopsin. *FEBS Lett.* **261,** 449–454 (1990).
22. Abrahams, J. P., Leslie, A. G. W., Lutter, R. & Walker, J. E. Structure at 2.8 Å resolution of F_1-ATPase from bovine heart mitochondria. *Nature* **370,** 621–628 (1994).
23. Koshland, D. E. Jr The structural basis of negative cooperativity: receptors and enzymes. *Curr. Opin. Struct. Biol.* **6,** 757–761 (1996).
24. Klostermeier, D., Seidel, R. & Reinstein, J. Functional properties of the molecular chaperone DnaK from *Thermus thermophilus*. *J. Mol. Biol.* **279,** 841–853 (1998).
25. Hohenfeld, I. P., Wegener, A. A. & Engelhard, M. Purification of histidine tagged bacteriorhodopsin, *pharaonis* halorhodopsin and *pharaonis* sensory rhodopsin II functionally expressed in *Escherichia coli*. *FEBS Lett.* **442,** 198–202 (1999).
26. Shimono, K., Iwamoto, M., Sumi, M. & Kamo, N. Functional expression of pharaonis phoborhodopsin in *Escherichia coli*. *FEBS Lett.* **420,** 54–56 (1997).
27. Leslie, A. G. W. Recent changes to the MOSFLM package for processing film and image data. *CCP4 ESF-EACMB Newslett. Protein Crystallogr.* **26 (2002).**
28. Collaborative Computational Project The CCP4 suite: programs for protein crystallography. *Acta Crystallogr. D* **50,** 760–763 (1994).
29. Brunger, A. T. *et al.* Crystallography & NMR system: a new software suite for macromolecular structure determination. *Acta Crystallogr. D* **54,** 905–921 (1998).
30. Jones, T. A., Zou, J. Y., Cowan, S. W. & Kjeldgaard, M. Improved methods for building protein models in electron-density maps and the location of errors in these models. *Acta Crystallogr. A* **47,** 110–119 (1991).
31. Kim, K. K., Yokota, H. & Kim, S. H. Four-helical-bundle structure of the cytoplasmic domain of a serine chemotaxis receptor. *Nature* **400,** 787–792 (1999).

Acknowledgements

We thank C. Baeken, I. Ritter and M. Schumacher for technical help, and B. Gehrmann for secretarial assistance. Discussions with R. G. Goody are gratefully acknowledged. We also thank the support by the staff of beamline ID14-1, and in particular E. Mitchell, ESRF, Grenoble, France; H. J. Brandt and C. Wandrey (IBT-Jülich) for a high yield fermentation of SRII containing *E. coli* cells; A. K. Islamov, A. I. Kuklin and G.N. Bobarikina for help in investigations on mechanisms of membrane protein crystallization in lipidic phases; and I. N. Groznov and V. B. Kireev for their support of this work. This study was supported by the Deutsche Forschungsgemeinschaft, the Max-Planck-Gesellschaft, and the Alexander von Humboldt Foundation.

Competing interests statement

The authors declare that they have no competing financial interests.

Correspondence and requests for materials should be addressed to G.B. (e-mail: g.bueldt@fz-juelich.de) or M.E. (e-mail: martin.engelhard@mpi-dortmund.mpg.de).

Coordinates have been deposited with the Research Collaboratory for Structural Bioinformatics Protein Data Bank under accession code 1H2S.

correction

Chromosome-wide SNPs reveal an ancient origin for *Plasmodium falciparum*

Jianbing Mu, Junhui Duan, Kateryna D. Makova, Deirdre A. Joy, Chuong Q. Huynh, Oralee H. Branch, Wen-Hsiung Li & Xin-zhuan Su

Nature **418**, 323–326 (2002).

It has been drawn to our attention that the 3D7 parasite, labelled as an African parasite in our Letter, was initially isolated from The Netherlands, although we have some genetic evidence suggesting an African origin (Wootton, J.C. and Su, X., manuscript in preparation). Therefore, 3D7 in our paper should be labelled as having a European origin, with a good probability of having originated from Africa. □